



CHORUS

This is the accepted manuscript made available via CHORUS. The article has been published as:

Role of commensurability of spin order for optical
magnetoelectric effect with electromagnons in multiferroic
 $\text{YMn}_{2}\text{O}_{5}$

R. Masuda, Y. Kaneko, Y. Yamasaki, Y. Tokura, and Y. Takahashi

Phys. Rev. B **96**, 041117 — Published 17 July 2017

DOI: [10.1103/PhysRevB.96.041117](https://doi.org/10.1103/PhysRevB.96.041117)

**Role of commensurability of spin orders for optical
magnetoelectric effect with electromagnons on multiferroic
YMn₂O₅**

R. Masuda,¹ Y. Kaneko,² Y. Yamasaki,^{1,2} Y. Tokura,^{1,2} and Y. Takahashi^{1,2,3}

¹*Department of Applied Physics and Quantum Phase Electronics Center (QPEC),
University of Tokyo, Tokyo 113-8656, Japan*

²*RIKEN Center for Emergent Matter Science (CEMS), Wako 351-0198, Japan*

³*PRESTO, Japan Science and Technology Agency, Chiyoda, Tokyo 102-8666, Japan.*

(Dated: June 19, 2017)

Abstract

Optical magnetoelectric effect, which produces the nonreciprocal directional dichroism, on the electromagnon resonances is investigated for multiferroic phases of YMn₂O₅ by terahertz spectroscopy. For the electromagnon driven by the exchange striction, a crucial role of the commensurability of spin order in the magnetoelectric coupling is manifested by the suppression of the directional dichroism in the incommensurate spin phase. Furthermore, the gapped electromagnon via the spin-current mechanism is identified in term of the directional dichroism, being irrespective of commensurability/incommensurability in the cycloidal spin order.

PACS numbers: 75.80.+q, 75.40.Gb, 75.85.+t, 76.50.+g

Magnetoelectric (ME) coupling in condensed matter has been attracting much attentions in versatile research areas including multiferroics [1–5], spintronics [5–7] as well as topological insulators [8, 9]. Unique ME coupling has been exemplified in multiferroics, in which the ferroelectricity is driven by the spin interactions, such as the exchange striction (ES) and the spin-current (SC) or inverse Dzyaloshinskii-Moriya mechanisms [4]. Specific topologies of both lattice and spin orders are necessary for the ferroelectricity driven by the ES, in which at least the commensurate magnetic modulation vector is indispensable. On the other hand, the SC mechanism gives rise to the electric polarization irrespective of the underlying lattice symmetry; the local electric polarization is expressed by $e_{ij} \times (S_i \times S_j)$, where the e_{ij} denotes the unit vector connecting adjacent spins S_i and S_j [10–12]. Accordingly, the cycloidal spin orders produce the macroscopic electric polarization, *i.e.* ferroelectricity, irrespective of commensurability/incommensurability in the spin order.

Multiferroics possesses unique fundamental spin excitations, referred to as electromagnon, which is a fluctuation of the spin orders endowed with electric activity. In fact, the electromagnon resonances driven by the ES and the SC mechanisms have been reported for many multiferroics [4, 13–15]. Furthermore, the ME coupling inherent to the electromagnon resonance gives rise to an novel optical response, *i.e.* optical magnetoelectric (OME) effect. The OME effect is exemplified by a nonreciprocal directional dichroism, which differentiates the optical responses for counter-propagating lights [16, 17]. The simultaneous breaking of the time-reversal and the space-inversion symmetries always allows the OME effect, so that the various optical transitions potentially show the OME effect as reported for multiferroics [15, 18–21], molecules [22] and artificial structures [23]. Because the OME effect is caused by an interference between the electric and magnetic transition dipoles, both electric and magnetic fields of light are responsible for the OME effect. For the electromagnon, the wavenumber (q) of magnon is essential for the OME effect, because the response to the uniform magnetic field is ensured at the magnetic Γ -point $q = q_m$ (q_m is a magnetic modulation vector) and $q = 0$, while the electromagnon has different selection rules on the wavenumber. For example, the strong OME effects have been reported for the SC-driven electromagnon [15, 24, 25] and for the on-site local excitations [18–20], whose electric and magnetic transitions occur at the magnetic Γ -point. On the other hand, the electromagnon driven by the ES has a more complex character because of the indispensable correlation with the underlying-lattice symmetry; the magnon branch is folded owing to the chemical

lattice structure [13, 26–29]. In addition, the noncollinear spin structure is responsible for this electromagnon. The resultant electromagnon excitation has a wavenumber being commensurate with the lattice. Thus the ES-driven electromagnon shows no magnetic activity and hence least OME effect, while showing the rather robust electric response.

Series of RMn_2O_5 (R =rare earth, Y, Bi) provides the abundant ME coupling for the spin-driven ferroelectricity as well as for the excitations including electromagnon [14, 26, 30–32]. The ferroelectric polarizations via the ES and the SC mechanisms coexist in the commensurate spin phase (CM), while the SC mechanism is solely responsible for the ferroelectricity in the incommensurate spin phase (ICM) [33–35]. Both CM and ICM phases exhibit strong electromagnon resonance, whose dominant peaks have been attributed to the ES driven one [26, 28].

In this letter, we report the OME effect on the electromagnon resonance in multiferroic YMn_2O_5 . The indispensable role of the commensurability for the OME effect on the ES-driven electromagnon is revealed. On the other hand, the electromagnon driven by the SC, not ES, mechanism is found to cause the OME effect irrespective of the commensurability/incommensurability of spin orders.

The single crystal of YMn_2O_5 was synthesized by the flux method. The ab plane sample with diameter of 2.3 mm and thickness of 800 μm was prepared. To obtain the optical constant in terahertz region, the terahertz time-domain spectroscopy in a transmission geometry was employed [36]. The femtosecond laser pulse from Ti:Sapphire laser was divided into two paths and focused on a bow-tie shaped antenna and dipole antenna to generate and detect terahertz pulses, respectively. The magnetic field of 7 T was applied along the a axis of the sample (Voigt geometry) during the measurement. To obtain the single ferroelectric domain, the electric field of 1.3 kV/cm was applied along the b axis while cooling the sample. The optical measurement was done without dc electric field. The pyroelectric current was measured under the constant electric field of 1.3 kV/cm [37].

YMn_2O_5 has orthorhombic crystal structure composed of $Mn^{3+}O_5$ pyramid and $Mn^{4+}O_6$ octahedron (Fig. 1 (a)). The spins on Mn^{3+} and Mn^{4+} ions form a long range magnetic order below $T_N \sim 45$ K; the zigzag chains along the b axis (solid green line in Fig. 1(a)) and the straight chains along the c axis consists of spins on Mn^{4+} sites (Fig. 1(b)). In the intermediate CM phase (19 K-41 K) with $q_m=(1/2, 0, 1/4)$, the spins in zigzag chains show an up-up-down sequence, resulting in the ferroelectric polarization ($P_{ES} \parallel b$) by ES (Fig.

1(a)) [32, 38]. On the other hand, the spin-cycloid structure along the c axis induces the local electric polarization (\mathbf{p}) canted from the a axis due to the SC mechanism (Fig. 1(a) and (b)). Ferroic b axis components of \mathbf{p} give rise to the ferroelectricity ($P_{\text{SC}} \parallel b$), whereas the a axis components of \mathbf{p} are canceled out due to the antiferroelectric order [34]. These different ferroelectric polarizations, P_{ES} and P_{SC} , are opposite to each other (Fig. 1(a) and inset to 1(c)), resulting in the total polarization $P = P_{\text{ES}} - P_{\text{SC}}$ [35]. The phase transition from CM to ICM phases occurs at $T_{\text{ICM}} \sim 19$ K with a jump of q_m to incommensurate one $q_m = (0.48, 0, 0.288)$ [32]. Since the ES mechanism cannot produce the net electric polarization in the ICM phase, the sudden drop of ferroelectric polarization is observed on the phase transition (inset to Fig. 1(c)). Accordingly, the P_{SC} solely constitutes the ferroelectricity in the ICM phase [34, 35].

The electromagnon resonances has been reported in the ferroelectric CM and ICM phases [14]. Figure 1(c) shows the extinction coefficient κ for $E^\omega \parallel b, H^\omega \parallel a$ under the magnetic field parallel to the a axis (7 T). In the ICM phase (16 K), three distinct peaks show up at 1.1 meV, 1.9 meV and 2.6 meV, which have been ascribed to the electromagnons driven by ES [14, 26, 28]. A modest peak around 3.7 meV (later referred to as mode I; see also Fig. 2) is also discerned. In the CM phase (21 K), three peaks are observed around 1.2 meV, 2.3 meV and 3.5 meV, while the spectra of the electromagnon resonances are broadened. At 41 K (paraelectric 1D-ICM phase), the broad absorption is seen. On the other hand, for $E^\omega \parallel a, H^\omega \parallel b$, no significant peaks are observed, except for a tiny magnon resonance at 2.7 meV at 4 K (Fig. 1(d)). Thus, the electromagnon is polarized parallel to the b axis, similar with the P [14].

Coexistence of ferroelectric polarization P and the magnetization M allows the OME effect, *i.e.* directional dichroism, for the light propagating parallel or antiparallel to $P \times M$ (Fig. 2(a)). The sign of the directional dichroism is changed by the reversal of P or M , as well as by the reversal of propagation vector of light (k^ω), so that the sign of $k^\omega \cdot (P \times M)$ determines the sign of directional dichroism [17]. When the k^ω is fixed in one direction, the sign of directional dichroism is expressed by the sign of $P \times M$ (Fig. 2(a)). Since the ferroelectric polarization is always parallel to the b axis, the magnetic field is applied along the a axis. The resultant point group $m'm2'$ allows the off-diagonal elements of first-order ME tensor including α_{ab} and α_{ba} , which are responsible for the OME effect [15, 17]. Note that the Faraday rotation, which is derived from the off-diagonal elements of μ and ϵ , is

prohibited in this Voigt geometry.

Figures 2(b) and 2(e) show the extinction coefficient κ for four possible configurations ($\pm P, \pm M$) in the ICM phase (4 K) and the CM phase (21 K), respectively. In the ICM phase, the dominant peaks of electromagnons at 0.9 meV, 2.1 meV and 2.6 meV, which have been ascribed to the electromagnon driven by the ES mechanism, are independent of the sign of P and M (Fig. 2(b)), resulting in the absence of the OME effect. In contrast, the change of the spectra in accordance with the signs of $P \times M$ on the modest peak at 3.7 meV (mode I) evidences the presence of the OME effect. Hereafter, the different states in terms of the OME effect are denoted as $+k^\omega$ for $P \times M > 0$ and $-k^\omega$ for $P \times M < 0$. The OME spectra $\Delta\kappa$ and the normalized OME spectra $\Delta\kappa/\kappa_0$ are defined by $\Delta\kappa = \kappa(+k^\omega) - \kappa(-k^\omega)$ and $\kappa_0 = (\kappa(+k^\omega) + \kappa(-k^\omega))/2$. The presence of the OME effect on the mode I is also indicated by a peak structure in the OME spectra $\Delta\kappa$ (Fig. 2(c)) as well as in the normalized OME spectra $\Delta\kappa/\kappa_0$ (Fig. 2(d)). The change of the extinction coefficient by the OME effect is as large as 13 % as shown in Fig. 2(d). Other lower-lying electromagnons show no significant OME effect as manifested by a negligible amount of $\Delta\kappa$ and $\Delta\kappa/\kappa_0$ below 3 meV in contrast to the fairly large peak intensities of parent resonances (Fig. 2 (b)).

The OME effect shows contrastive behaviors in the intermediate CM phase. The directional dichroism is observed in a broad energy range below 5 meV as manifested by the change of κ in accord with the sign of $P \times M$ (Fig. 2(e)). The OME spectra ($\Delta\kappa$) and the normalized one ($\Delta\kappa/\kappa_0$) at 21 K are composed of three pronounced peaks; lower-lying peaks at 1 meV (mode II) and at 2.5 meV (mode III) show positive sign, while the mode I at 3.7 meV has negative sign.

Since the OME effect is derived from the first-order ME effect, the linear magnetic field dependence is expected. In fact, the monotonous increase of the OME effect is observed for the normalized OME spectra (Fig. 3(a)) and for the peak intensities of modes I, II and III (Fig. 3(b)) with increasing the magnetic field.

Figures 3 (c) and 3(d) show the temperature dependence of the normalized OME spectra ($\Delta\kappa/\kappa_0$). The temperature dependence of peak intensities of the normalized OME effect for the modes I, II and III is summarized in Figs. 4(a) and 4(b). The OME effect on the mode I decreases with increasing temperature in the ICM phase (4 K-18 K), and shows a sudden jump to negative sign upon the phase transition to CM phases (at ~ 19 K) as shows in Fig. 4(a) . On the other hand, the modes II and III exhibit the distinct OME effect only in the

CM phase. These results implies that the commensurability of spin orders is relevant to the OME effect on electromagnon.

The spectral weight of the electromagnon (SW) is defined by the integration of optical conductivity $\sigma(\omega)$ from 1 meV to 5 meV. The spectral weight of the OME effect (Δ SW) is defined here by the absolute value of the change of optical conductivity; Δ SW = $\int_{1\text{meV}}^{5\text{meV}} |\sigma(\omega, +k^\omega) - \sigma(\omega, -k^\omega)| d\omega$. The SW shows monotonous increase with decreasing temperature (Fig. 4(c)). (Note that the slight decrease of SW in the ICM phase may be caused by the energy shift of the strong peak below our measurement range of SW (1-5 meV).) On the other hand, the OME effect (Δ SW) becomes maximum in the CM phase and suddenly drops upon the phase transition to the ICM phase (Fig. 4(d)). This sudden drop is caused by the suppression of OME effect on the mode II and III. The residual OME effect reflects the appreciable Δ SW for the mode I in the ICM phase.

The enhancement of the OME effect in the CM phase suggests the contribution from the ES mechanism. The ES mechanism gives rise to the ferroelectricity only in the CM phase, whereas the cancellation of microscopic polarizations results in the absence of net polarization for the ICM phase. In contrast, the electromagnon resonance is generated by the ES mechanism irrespective of commensurability or incommensurability as reported for RMn_2O_5 and perovskite $RMnO_3$ [13, 14]. To induce the OME effect on the ES-driven electromagnon, the magnetic activity is indispensable in addition to the electric activity. Oscillation of the uniform magnetic field induces the magnon excitation at $q = q_m$ and $q = 0$. Since the ES-driven electromagnon is the magnon with commensurate wavenumber, the ES-driven electromagnon potentially possesses the magnetic activity only when the q_m is commensurate. In fact, the modes II and III, which can be ascribed to the ES-driven electromagnon, show the OME effect in the CM phase (Figs. 3(d) and 4(a)), indicating their character responding to the magnetic field of light. These electromagnons lose the magnetic response in the ICM phase, resulting in the absence of the OME effect (Figs. 3(c) and 4(a)).

The OME effect on the mode I in the ICM phase suggests that the SC mechanism causes this electromagnon, which has both electric and magnetic activities irrespective of commensurability/incommensurability of the cycloidal spin order. The spin-cycloid structure on the Mn^{4+} chains (Fig. 1(b)) generates the local electric polarization \mathbf{p} , so that the uniform electric field perpendicular to \mathbf{p} cause the fluctuation of \mathbf{p} , resulting in the electromagnon

with the character of the rotational oscillation of spin-cycloid plane [39]. In the YMn_2O_5 , two spin-cycloid chains are contained in the unit cell, whose polarization \mathbf{p} along the a axis is canceled out owing to the antiferroelectric order (Fig. 1(a)) [34]. These hidden polarizations, however, potentially lead to the electromagnon excitation polarized perpendicular to the spin-plane ($E^\omega \parallel b$), resulting in the anti-phase rotational oscillation of \mathbf{p} , *i.e.* flapping of the spin-cycloid planes (Fig. 4(c)). Because of the optical-mode character for the anti-phase rotational oscillation, this SC driven electromagnon should have an intrinsic energy gap as observed here. This is consistent with the observed magnon dispersion in YMn_2O_5 [28], in which a certain amount of weight has been observed around the resonance energy of mode I (~ 3.7 meV) on the magnetic Γ -point. It is worth noting that the SC-driven electromagnon is ascribed to the Nambu-Goldstone mode for the single spin-cycloid chain, resulting in the gapless excitation [39]. In fact, the lower resonance energy has been reported for the SC-driven electromagnon on the perovskite RMnO_3 [15, 24].

The other difference from the single spin-cycloid is the configuration of the magnetic field necessary for the OME effect. It is known that the magnetic field perpendicular to the spin-plane induces OME effect as shown for the case of the perovskite RMnO_3 [15]. In the present compound, however, the local magnetic-moments \mathbf{m} induced by the magnetic field perpendicular to the spin-plane ($H_{dc} \parallel b$) result in the opposite sign of the $\mathbf{p} \times \mathbf{m}$ for each chain (Fig. 4(d)), so that the OME effect are canceled out. In contrast, the magnetic field along the a axis causes the same sign of $\mathbf{p} \times \mathbf{m}$ for each canted spin-cycloid (Fig. 4(c)), resulting in the OME effect on the electromagnon (mode I).

The sign change of the OME effects on the mode I can be explained by the correlation between the net polarization P and P_{SC} (Fig. 4(a)), consistently with the above assignment to the OME electromagnon; the direction of the P_{SC} is antiparallel to the net polarization $P(= P_{\text{ES}} - P_{\text{SC}})$ in the CM phase and parallel to $P(= P_{\text{SC}})$ in the ICM phase [35, 37] (see inset to Fig. 1(c)). Thus the reversal of the P_{SC} occurs on the phase transition from ICM to CM phases, while keeping the sign of net polarization P . Accordingly, the sign of $P_{\text{SC}} \times M$ for the internal spin-cycloid chains is reversed, resulting in the reversal of the OME effect for the mode I as demonstrated in Fig. 4(a).

In conclusion, we have investigated the OME effect on the electromagnon resonance driven by the ES and the SC mechanisms in multiferroic YMn_2O_5 by terahertz spectroscopy. The OME effect was observed as manifested by the nonreciprocal directional dichroism in the

spin-driven ferroelectric phases. The enhancement of the OME effect with additional peaks in the CM phase indicates the indispensable role of commensurability for the OME effect on the ES-driven electromagnon. The electromagnon driven by the SC mechanism, whose resonance energy is gapped due to the character of optical mode, is identified in terms of the OME effect being irrespective of the commensurability/incommensurability in the spin-cycloid.

-
- [1] T. Kimura, T. Goto, H. Shintani, K. Ishizaka, T. Arima and Y. Tokura, *Nature (London)* **426**, 55 (2003).
 - [2] W. Eerenstein, N. D. Mathur and J. F. Scott, *Nature (London)* **442**, 759 (2006).
 - [3] J. F. Scott, *Science* **315**, 954959 (2007).
 - [4] Y. Tokura, S. Seki and N. Nagaosa, *Rep. Prog. Phys.* **77**, 076501 (2014).
 - [5] F. Matsukura, Y. Tokura and H. Ohno, *Nat. Nanotech.* **10**, 209 (2015).
 - [6] C. Chappert, A. Fert and F. Nguyen Van Dau, *Nature Mater.* **6**, 813 (2007).
 - [7] V. Garcia, M. Bibes, L. Bocher, S. Valencia, F. Kronast, A. Crassous, X. Moya, S. Enouz-Vedrenne, A. Gloter, D. Imhoff, C. Deranlot, N. D. Mathur, S. Fusil, K. Bouzehouane, A. Barthlmy, *Science* **26**, 1106 (2010).
 - [8] A. M. Essin, J. E. Moore and D. Vanderbilt, *Phys. Rev. Lett.* **102**, 146805 (2009).
 - [9] X.-L. Qi., R. Li, J. Zang and S.-C. Zhang, *Science* **323**, 1184 (2013).
 - [10] H. Katsura, N. Nagaosa and A. V. Balatsky, *Phys. Rev. Lett.* **95**, 057205 (2005).
 - [11] M. Mostovoy, *Phys. Rev. Lett.* **96**, 067601 (2006).
 - [12] I. A. Sergienko and E. Dagotto, *Phys. Rev. B* **73**, 094434 (2006).
 - [13] A. Pimenov, A. A. Mukhin, V. Yu. Ivanov, V. D. Travkin, A. M. Balbashov and A. Loidl, *Nature Phys.* **2**, 97 (2006).
 - [14] A. B. Sushkov, R. V. Aguilar, S. Park, S-W. Cheong, and H. D. Drew, *Phys. Rev. Lett.* **98**, 027202 (2007).
 - [15] Y. Takahashi, R. Shimano, Y. Kaneko, H. Murakawa and Y. Tokura, *Nature Phys.* **8**, 121 (2012).
 - [16] L. D. Barron, *Molecular Light Scattering and Optical Activity* (Cambridge Univ. Press, 2004).
 - [17] T. Arima, *J. Phys. Condens. Matter* **20**, 434211 (2008).

- [18] M. Saito, K. Ishikawa, K. Taniguchi, and T. Arima, *Phys. Rev. Lett.* **101**, 117402 (2008).
- [19] M. Saito, K. Taniguchi and T. Arima, *J. Phys. Soc. Jpn* **77**, 013705 (2008).
- [20] I. Kézsmárki, N. Kida, H. Murakawa, S. Bordács, Y. Onose and Y. Tokura, *Phys. Rev. Lett.* **106**, 057403 (2011).
- [21] M. Kubota, T. Arima, Y. Kaneko, J. P. He, X. Z. Yu, and Y. Tokura, *Phys. Rev. Lett.* **92**, 137401 (2004).
- [22] G. L. J. A. Rikken, C. Strohm and P. Wyder, *Phys. Rev. Lett.* **89**, 133005 (2002).
- [23] N. Kida, H. Yamada, H. Sato, T. Arima, M. Kawasaki, H. Akoh, and Y. Tokura, *Phys. Rev. Lett.* **99**, 197404 (2007).
- [24] Y. Takahashi, Y. Yamasaki, and Y. Tokura, *Phys. Rev. Lett.* **111**, 037204 (2013).
- [25] S. Kibayashi, Y. Takahashi, S. Seki, and Y. Tokura, *Nat. Commun.* **5**, 4583 (2014).
- [26] A. B. Sushkov, M. Mostovoy, R. V. Aguilar, S. -W. Cheong, and H. D. Drew: *J. Phys. Condens. Matter* **20**, 434210 (2008).
- [27] R. Valdés Aguilar, M. Mostovoy, A. B. Sushkov, C. L. Zhang, Y. J. Choi, S-W. Cheong and H. D. Drew, *Phys. Rev. Lett.* **102**, 047203 (2009).
- [28] J.-H. Kim, M. A. van der Vegte, A. Scaramucci, S. Artyukhin, J.-H. Chung, S. Park, S-W. Cheong, M. Mostovoy, and S.-H. Lee, *Phys. Rev. Lett.* **107**, 097401 (2011).
- [29] N. Kida, D. Okuyama, S. Ishiwata, Y. Taguchi, R. Shimano, K. Iwasa, T. Arima, and Y. Tokura, *Phys. Rev. B* **80**, 220406(R) (2009).
- [30] A. Inomata and K. Kohn, *J. Phys. Condens. Matter* **8**, 2673 (1996).
- [31] N. Hur, S. Park, P. A. Sharma, J. S. Ahn, S. Guha, and S.-W. Cheong, *Nature (London)* **429**, 392 (2004).
- [32] Y. Noda, H. Kimura, M. Fukunaga, S. Kobayashi, I. Kagomiya, and K. Kohn, *J. Phys. Condens. Matter.* **20**, 434206 (2008).
- [33] L. C. Chapon, P. G. Radaelli, G. R. Blake, S. Park, and S.-W. Cheong, *Phys. Rev. Lett.* **96**, 097601 (2006).
- [34] J.-H. Kim, S.-H. Lee, S. I. Park, M. Kenzelmann, A. B. Harris, J. Schefer, J.-H. Chung, C. F. Majkrzak, M. Takeda, S. Wakimoto, S. Y. Park, S-W. Cheong, M. Matsuda, H. Kimura, Y. Noda, and K. Kakurai, *Phys. Rev. B* **78**, 245115 (2008).
- [35] S. Wakimoto, H. Kimura, Y. Sakamoto, M. Fukunaga, Y. Noda, M. Takeda, and K. Kakurai, *Phys. Rev. B* **88**, 140403(R) (2013).

- [36] N. Kida, Y. Ikebe, Y. Takahashi, J. P. He, Y. Kaneko, Y. Yamasaki, R. Shimano, T. Arima, N. Nagaosa and Y. Tokura, Phys. Rev. B **78**, 104414 (2008).
- [37] M. Fukunaga and Y. Noda, J. Phys. Soc. Jpn. **79**, 054705 (2010).
- [38] S. Kobayashi, T. Osawa, H. Kimura, Y. Noda, I. Kagomiya and K. Kohn, J. Phys. Soc. Jpn. **73**, 1593 (2004).
- [39] H. Katsura, A. V. Balatsky and N. Nagaosa, Phys. Rev. Lett. **98**, 027203 (2007).

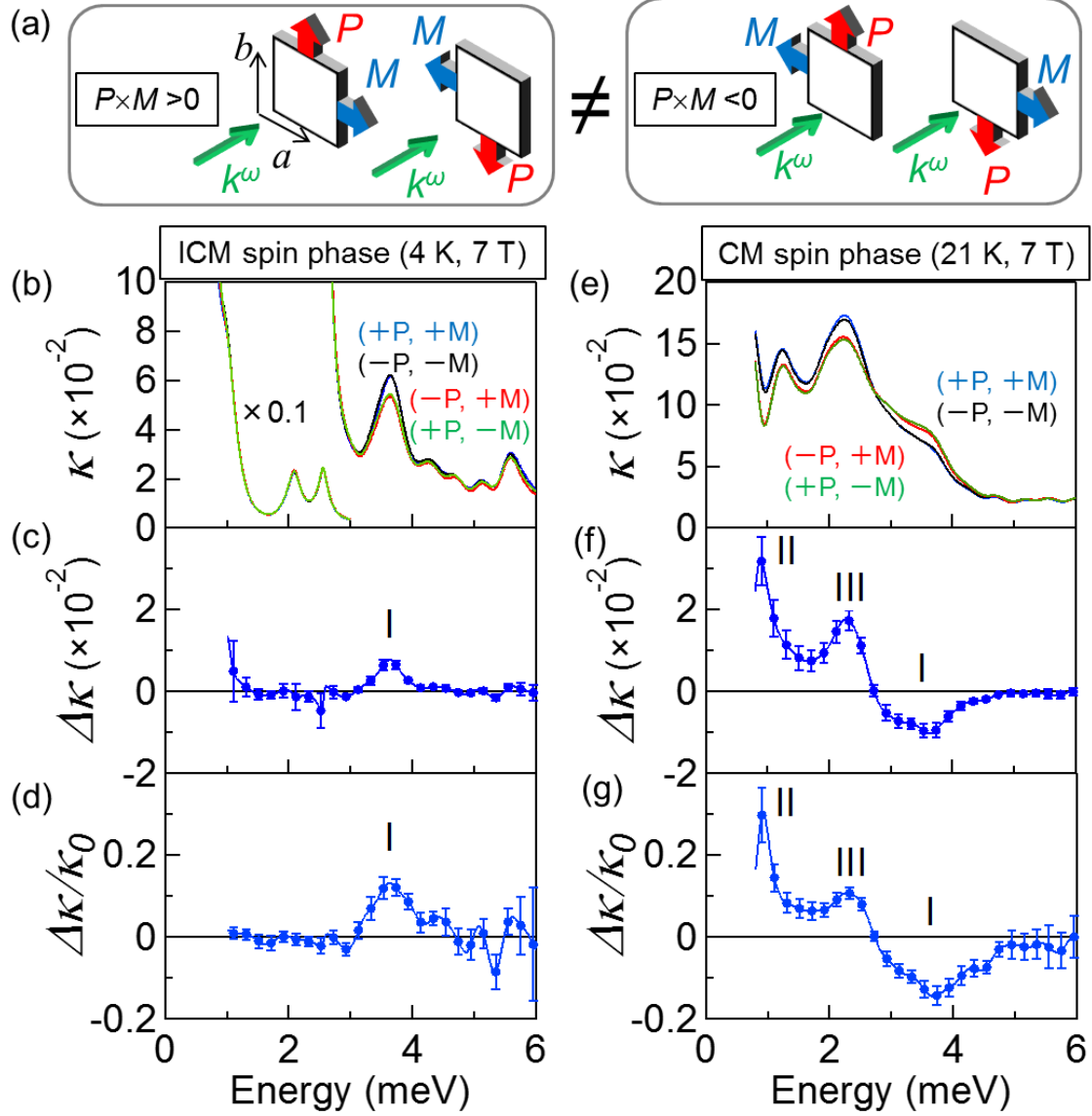


FIG. 2: (color online)(a) Configurations of P , M , and k^ω and their relation in the OME effect. Spectra of κ (b) in the ICM phase (4 K) and (e) in the CM phase (21 K). The signs of P and M for the respective spectra are indicated. The OME spectra ($\Delta\kappa$) and the normalized OME spectra ($\Delta\kappa/\kappa_0$) for the ICM phase (c-d) and for the CM phase (f-g). (see the text for definitions of $\Delta\kappa$ and $\Delta\kappa/\kappa_0$.) The magnetic field of 7 T is applied along the a axis.

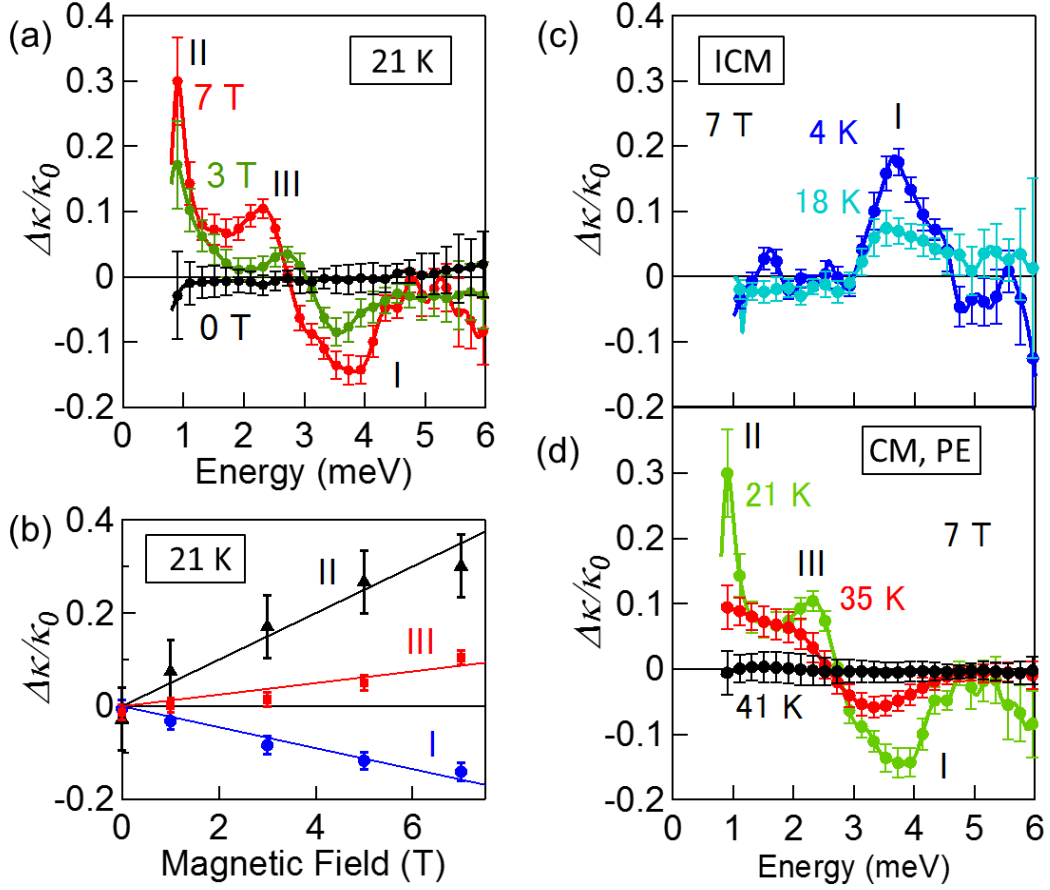


FIG. 3: (color online) The magnetic field ($H_{dc} \parallel a$) dependence of (a) the normalized OME spectra ($\Delta\kappa/\kappa_0$) and (b) the peak intensities for the modes I, II and III in the CM phase (21 K). (Lines are guide to eye.) The temperature dependence of the normalized OME spectra (c) in the ICM phase and (d) in the CM and paraelectric (1D-ICM) phases.

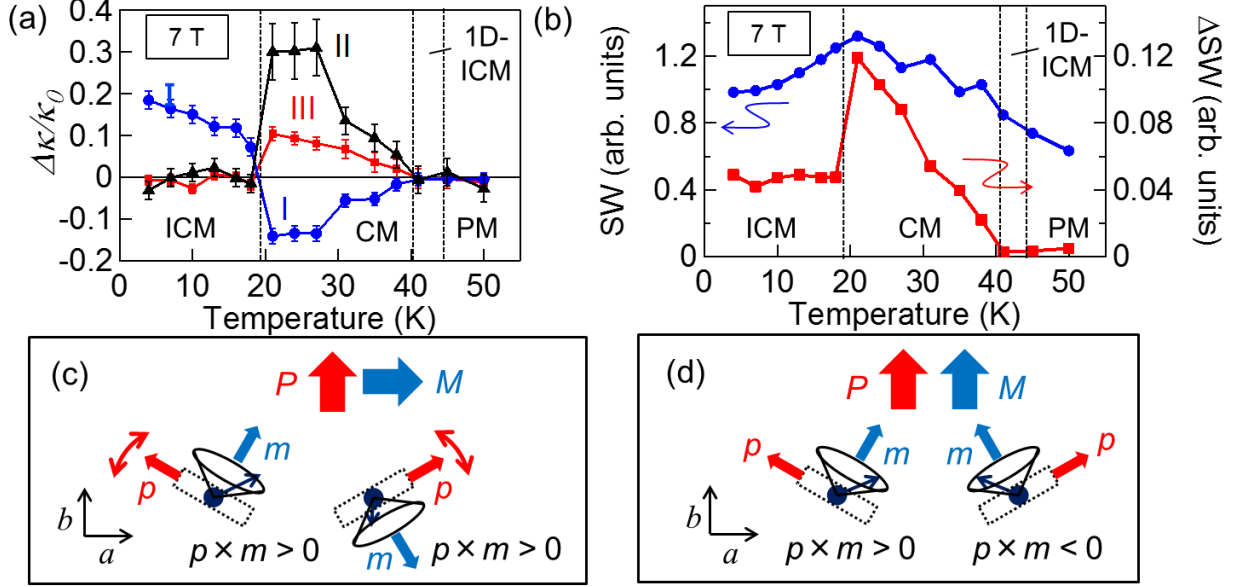


FIG. 4: (color online) (a) Temperature dependences of peak intensities of the normalized OME effect $\Delta\kappa/\kappa_0$ for modes I, II and III (see Figs. 3(c) and 3(d)). (b) Temperature dependences of the spectral weights of the electromagnon (SW) and the OME effect (ΔSW). (see the text for definitions.) The magnetic field of 7 T is applied along the a axis. The side view of the two spin-cycloid chains on Mn^{4+} (see Figs. 1(a) and 1(b)) under the magnetic field (c) $H_{dc} \parallel a$ and (e) $H_{dc} \parallel b$. The spin-plane motion for the mode I ascribed to the SC-driven electromagnon is shown in (c).